Available online at www.sciencedirect.com
SCIENCE DIRECT
Biomaterials 27 (2006) 3904–3911
Biomaterials
www.elsevier.com/locate/biomaterials

Bioactivity and cytocompatibility of zirconia (ZrO_2) films fabricated by cathodic arc deposition

Xuanyong Liu[a,b,c,*], Anping Huang[a], Chuanxian Ding[b], Paul K. Chu[a,*]

[a]*Department of Physics and Materials Science, City University of Hong Kong, Tat Chee Avenue, Kowloon, Hong Kong*
[b]*Shanghai Institute of Ceramics, Chinese Academy of Sciences, 1295 Dingxi Road, Shanghai 200050, China*
[c]*College of Materials Science and Engineering, Hunan University, Changsha 410082, China*

Received 16 November 2005; accepted 1 March 2006
Available online 27 March 2006

Abstract

Zirconium oxide thin films were fabricated on silicon wafers using a filtered cathodic arc system in concert with oxygen plasma. The structure and phase composition of the zirconium oxide thin films were characterized by atomic force microscopy (AFM), X-ray diffraction (XRD), Rutherford backscattering spectrometry (RBS), and transmission electron microscopy (TEM). The bioactivity was assessed by investigating the formation of apatite on the film surface after soaking in simulated body fluids. Bone marrow mesenchymal stem cells (BMMSC) were used to further evaluate the cytocompatibility of the materials. The results indicate that the films are composed of stoichiometric ZrO_2 and the composition is quite uniform throughout the thickness. Bone-like apatite can be formed on the surface of the ZrO_2 thin film in our SBF immersion experiments, suggesting that the surface is bioactive. The outermost layer of the ZrO_2 thin film comprises nano-sized particles that can be identified by AFM images taken on the thin film surface and TEM micrographs obtained from the interface between the ZrO_2 thin film and apatite layer. The nanostructured surface is believed to be the key factor that apatite is induced to precipitate on the surface. Bone marrow mesenchymal stem cells are observed to grow and proliferate in good states on the film surface. Our results show that ZrO_2 thin films fabricated by cathodic arc deposition exhibit favorable bioactivity and cytocompatibility.

Keywords: ZrO_2 thin film; Cathodic arc deposition; Bioactivity; Apatite

1. Introduction

Good chemical and dimensional stability, mechanical strength, toughness, and Young's modulus similar to that of stainless steel alloys make zirconia excellent ceramic biomaterials. The first paper concerning biomedical applications of zirconia was published in 1969 and the use of zirconia in the ball heads of total hip replacements (THR) was introduced in 1988 [1]. This application remains one of the current main applications of zirconia. Nowadays, more than 600,000 zirconia femoral heads have been implanted worldwide, mainly in the US and Europe [2]. The requirements for zirconia ceramic implants are described in the ISO standard No. 13356 [3]. In order to improve the wear and corrosion resistance, zirconia was also deposited onto metal implants using plasma-spraying technology [4,5]. Zirconia is, however, considered a bio-inert ceramic because when implanted, it only shows a morphological fixation with the surrounding tissues without producing any chemical or biological bonding. In order to improve the effects, bioactive materials such as bioactive glasses and hydroxyapatite have been coated onto or incorporated into zirconia to combine the favorable mechanical properties of this high-strength material with the bioactive properties of the coatings [6–10].

Induction of the apatite-forming ability on a nanocomposite of ceria-stabilized tetragonal zirconia polycrystals (Ce-TZP) and alumina (Al_2O_3) polycrystals via chemical treatments in aqueous solutions of H_3PO_4,

*Corresponding authors. Tel.: +86 852 2788724; fax: +86 852 27887830 (P.K. Chu); Tel.: +86 21 52414103; fax: +86 2152413903 (X. Liu).
E-mail addresses: xyliu@mail.sic.ac.cn (X. Liu), paul.chu@cityu.edu.hk (P.K. Chu).

0142-9612/$ - see front matter © 2006 Elsevier Ltd. All rights reserved.
doi:10.1016/j.biomaterials.2006.03.007

H_2SO_4, HCl, or NaOH has been investigated [11]. When this type of nano-composite is subjected to this treatment at 95 °C for 4 hours, Zr–OH groups that enhance the formation of apatite in simulated body fluids (SBF) are formed on the surface. The apatite-forming ability of zirconium metal pre-treated in $\geqslant 5$ M aqueous NaOH solutions has also been demonstrated in SBF immersion tests [12]. Apatite nucleation is believed to be induced by Zr–OH groups in a zirconia hydrogel layer that forms on the metal upon exposure to NaOH. The apatite-forming ability of NaOH-treated zirconium metal is, however, weaker than that of NaOH-treated titanium and tantalum metals. Uchida et al. [13] have shown that pure zirconia gel and zirconia gels containing sodium or calcium induce the formation of apatite in SBF only when they possess a tetragonal and/or a monoclinic structure. Zirconia is also considered an ideal candidate for immobilization of biomolecules with oxygen functional groups due to its thermal stability, chemical inertness, lack of toxicity [14], as well as affinity to these functional groups [15]. ZrO_2 thin films prepared by various methods have in fact been used to immobilize DNA in DNA biosensors [16,17].

In this work, ZrO_2 thin films were deposited on Si wafers using a cathodic arc plasma source in the presence of oxygen. The bioactivity and cytocompatibility of ZrO_2 thin films were evaluated using SBF soaking and cell culturing tests. The objective of this work is to investigate the mechanism of the induced bioactivity and potential application of the ZrO_2 thin films in hard tissue replacements.

2. Experimental details

The ZrO_2 thin films were fabricated on n-type, 100 mm Si (1 0 0) wafers using a filtered cathodic arc system [18]. The experimental apparatus used in this study included a magnetic duct and cathodic arc plasma source. A curved magnetic duct was inserted between the plasma source and main chamber to remove macro-particles produced in the cathodic arc plasma. The cathodes used in our experiments were 99.9% pure Zr rods with a diameter of 1 cm. The arc was ignited within a pulse duration of about 300 ms at a repetition rate of 60 Hz. The zirconium discharge was controlled by the main arc current between the cathode and anode. Oxygen gas was bled into the arc region and the mixed zirconium and oxygen plasma was guided into the vacuum chamber by an electromagnetic field applied to the curved duct. The duct was biased to −20 V to exert a lateral electric field while the external solenoid coils wrapped around the duct produced the axial magnetic field with a magnitude of 100 G. The substrate temperature that was controlled by a heating assembly mounted below the stainless steel substrate holder was measured by a chromel–alumel thermocouple attached to the backside of the Si substrate. Before deposition, the samples that were positioned about 15 cm away from the exit of the plasma stream were cleaned by argon plasma for 2 min using a sample bias of −500 V. The base pressure in the vacuum chamber was about 1×10^{-5} Torr and RF power of 100 W was applied for a deposition time of 120 min.

Rutherford backscattering spectrometry (RBS) was carried out using a 2 MeV $4He^{++}$ beam and a backscattering angle of 170° to determine the composition as well as thickness of the thin films. Contact mode atomic force microscopy (AFM) was conducted on a Park Scientific Instrument (PSI) Autoprobe Research System to evaluate the surface morphology over a scanned area of 2 μm × 2 μm. The microstructure of the thin films was determined by Fourier transform infrared (FTIR) spectroscopy using a PERKIN ELMER spectrometer and X-ray diffraction (XRD) using a Siemens D500/501 thin film diffractometer with a Cu K_α source.

After ultrasonically washed in acetone and rinsed in deionized water, the deposited samples were soaked in a simulated body fluid (SBF) for 28 days to investigate their bioactivity. The SBF solution was buffered at pH 7.4 with trimethanol aminomethane-HCl. The ionic concentrations in the solution are nearly equal to those in human body blood plasma [19]. The surface of the ZrO_2 thin films before and after the immersion test was observed by cold field emission scanning electron microscopy (SEM) using a JEOL JSM-6700F. Phase characterization of the newly-formed layer on the ZrO_2 thin film was conducted by X-ray diffraction (XRD) employing a JAPAN-RICOH diffractometer equipped with Ni-filtered Cu K_α radiation ($\lambda = 1.5418$ A). In the X-ray diffraction experiments, the incident beam angle was fixed at 2°. The functional groups in the newly-formed layer were determined by transmission-mode Fourier transform infrared (FTIR) spectroscopy using a Bio Rad FTS-185.

The cross-sectional views of the as-deposited and soaked ZrO_2 thin films were investigated by transmission electron microscopy (TEM) using a JEM2100F. Thinned samples were prepared to allow TEM examination using the following procedures. Two samples were first attached with the films facing each other and then cut into a 1 mm thick specimen. The specimen was then attached to a tripod polisher with glue and polished from both sides until the thickness became about 30 μm. Finally, the thickness of the specimen was further reduced employing a low-angle ion-thinning Precise Ion Polishing System (PIPS).

Bone marrow mesenchymal stem cells (BMMSC) were used to evaluate the biocompatibility of the ZrO_2 thin films. The cells were isolated from bone marrow of a healthy newborn calf femur, as described by Maniatopoulos et al. [20]. After the bone was sawed open, BMMSC were collected and cultured in a flask containing 10 ml Dulbecco's modified Eagle's medium-low glucose (Gibco) with 10% fetal calf serum plus antibiotics at 37 °C in a humidified atmosphere of 95% air and 5% CO_2. In this investigation, only the cells at the 3rd–5th passage were employed. The cells were seeded on each sample with a density of 2.5×10^4 cells/cm^2 in a 24-well plate and incubated for 3 days in a DMEM culture medium supplemented with 10% calf serum maintained at 37 °C in a humidified atmosphere of 95% air and 5% CO_2. After different culture times, the discs were removed from the culture wells and rinsed with a phosphate-buffered saline solution (pH 7.2, PBS) twice to remove unattached cells and fixed with 2.5% glutaraldehyde solution in a sodium cacodylate buffer (pH 7.40) for 30 min. Before SEM was performed, the samples were dehydrated in a grade ethanol series (30, 50, 75, 90, 95 and 100% v/v) for 10 min, respectively, with final dehydration conducted in absolute ethanol twice followed by drying in the hexamethyldisilizane (HMDS) ethanol solution series [21].

3. Results and discussion

The TEM and high-resolution TEM (HRTEM) micrographs taken near the ZrO_2 thin film and silicon substrate interface are depicted in Fig. 1. As shown in Fig. 1a, the thickness of the thin film is about 60 nm and the ZrO_2 thin film is polycrystalline. The (1 0 1) planes of the tetragonal ZrO_2 with a spacing of about 0.3 nm are well resolved in this area (Fig. 1b). An amorphous layer with a thickness of about 2 nm is observed at the interface between the Si wafer and ZrO_2 thin film. The amorphous layer is believed to be the transition layer encompassing Zr, O and Si because the weak absorption bands at around 720 cm^{-1} for Zr–O–Si and 800 and 1080 cm^{-1} for the Si–O vibration mode can be observed in the FTIR spectra acquired from the ZrO_2 thin films on silicon wafer [22], as shown in Fig. 2. The strong absorption peaks near 580, 510 and 420 cm^{-1}

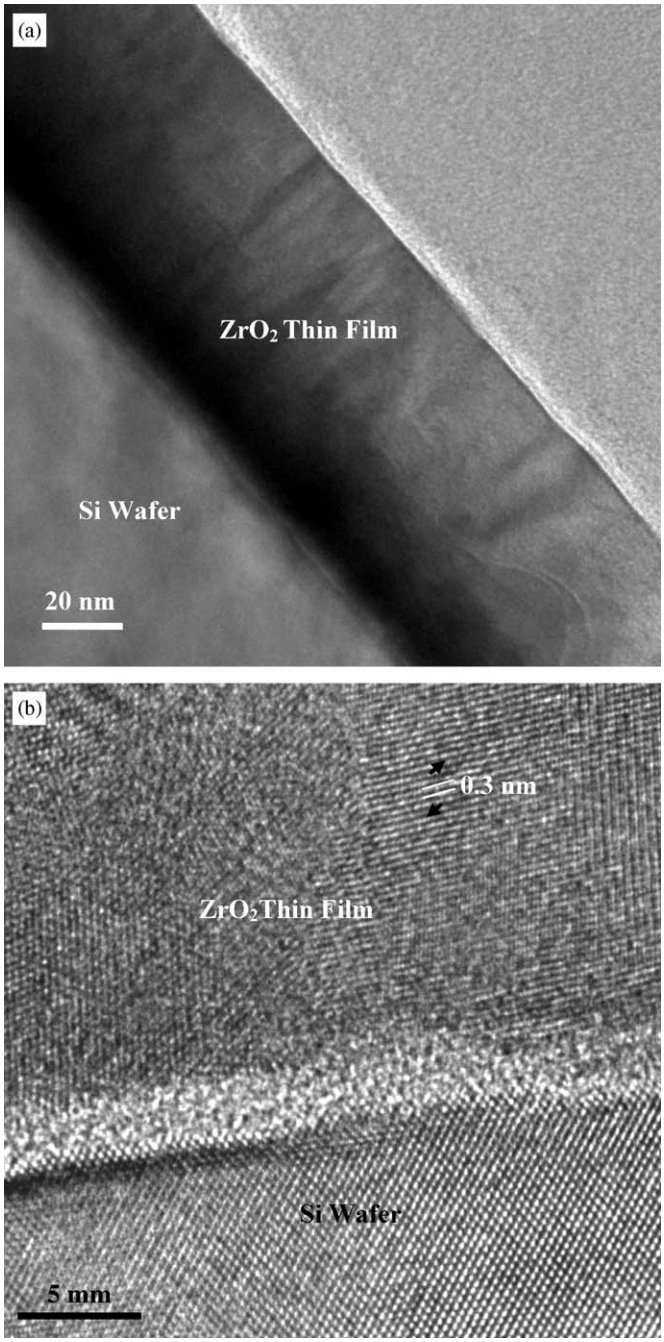

Fig. 1. (a) TEM picture and (b) high-resolution transmission electron microscopy (HRTEM) micrographs taken near the ZrO_2 thin film and silicon interface.

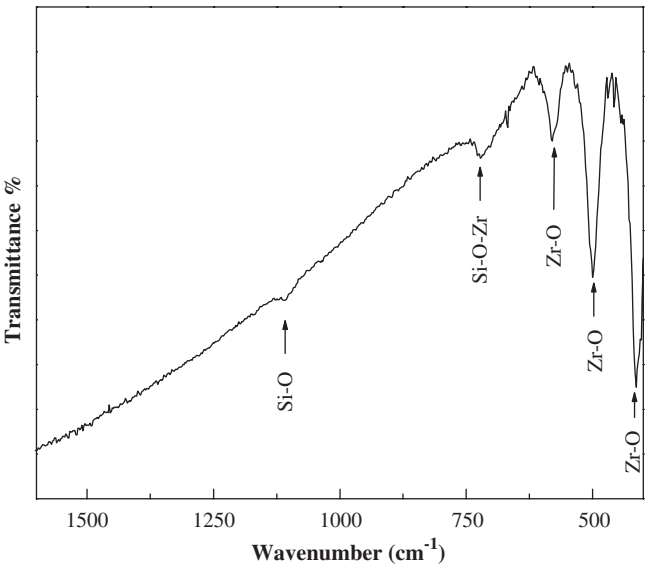

Fig. 2. FTIR spectrum of the ZrO_2 thin film on silicon wafer.

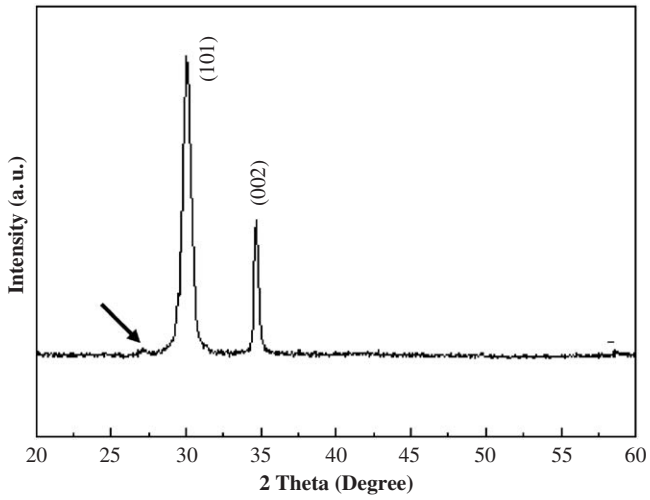

Fig. 3. Thin film-XRD pattern of the ZrO_2 thin film on silicon wafer.

corresponding to the Zr–O vibrational modes are also observed [23,24]. The XRD results shown in Fig. 3 disclose that the thin film is crystallized, as indicated by the diffraction peaks at 29.83° and 34.85° that can be attributed to, respectively, the (1 0 1) and (0 0 2) planes of the tetragonal ZrO_2 phase. A small peak which may be attributed to the (1 1 1) plane of the monoclinic phase can also be observed, as marked by the arrows in Fig. 3.

The surface microstructure of the as-deposited ZrO_2 thin film revealed by AFM and SEM are presented in Fig. 4. In the AFM results including the line profile (Fig. 4a), many nano-sized protuberances can be clearly observed. However, the line profile of the surface topography indicates that the surface of the film is very smooth, and its R_{max} (maximum roughness) value is smaller than 1 nm. This is further clarified by the high resolution SEM micrograph displayed in Fig. 4b. The surface is so smooth that we can hardly find any objects in the view at 100,000 × magnification. The protuberances observed on the AFM picture thus do not reflect surface roughness or individual grains, but rather convolution of the AFM data.

Fig. 5 displays the RBS spectrum that shows both the experimental and fitted results. The formation of stoichiometric ZrO_2 (Zr:O = 1:2) is indicated and the composition of the thin film is quite uniform throughout the thickness by deconvoluting the RBS data. This is thought to be in part due to the effective elimination of Zr macro-particles

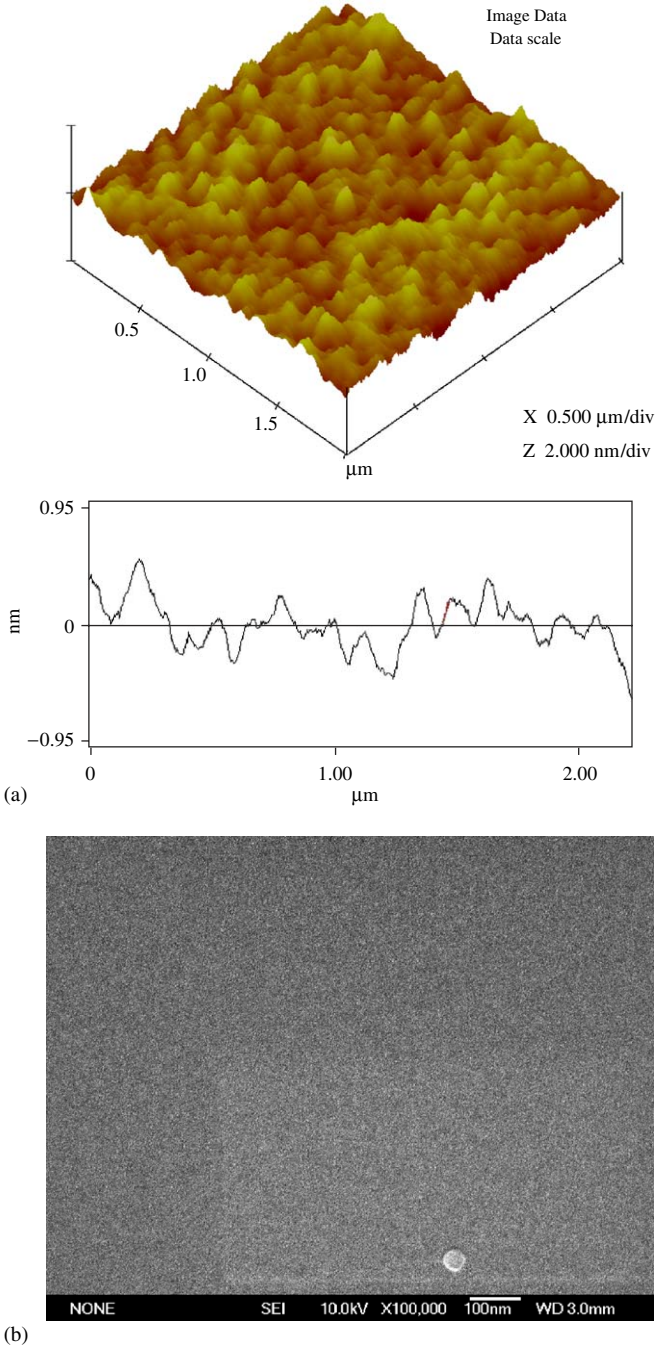

Fig. 4. Surface view of the ZrO_2 thin film obtained by: (a) AFM (including line scan) and (b) SEM.

formed in the cathodic arc by the curved magnetic filter. The process efficacy can be evaluated according to the simulation results of the zirconium contents in the layer [18].

Fig. 6 depicts the SEM plan views of the ZrO_2 thin films after soaking in SBF for 14 and 28 days. After 14 days, some single and clustered ball-like particles are formed on the ZrO_2 thin films (Fig. 6a). The surfaces of the thin films are, however, not covered completely. After 28 days, the number of these ball-like particles increases, and the surface is totally covered by the newly formed layer

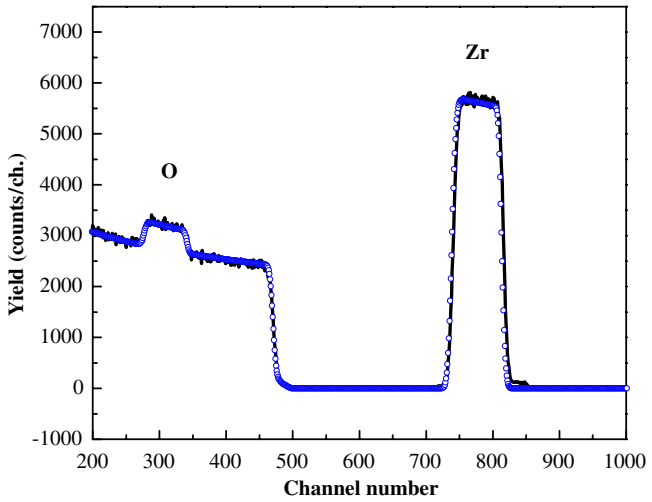

Fig. 5. RBS spectrum showing both the experimental and fitted results acquired from the ZrO_2 thin film.

(Fig. 6b). The higher magnification micrograph indicates that the ball-like particles are composed of many needle-like crystallites (Fig. 6c). The EDS spectra of the soaked ZrO_2 thin films are displayed in the top right corner of the respective SEM micrographs. The EDS spectra acquired from the ZrO_2 thin film soaked in SBF for 14 days reveal the existence of calcium and phosphorus on the surface. After immersion in SBF for 28 days, more calcium and phosphorus are detected indicating the formation of a denser and thicker Ca–P layer. The atomic ratios of Ca to P calculated from the EDS spectra of the ZrO_2 thin film soaked in SBF for 14 and 28 days are about 1.15 and 1.48, respectively. Our data show that the atomic ratio of Ca to P in the Ca–P layer increases gradually to that of hydroxyapatite (1.67) with longer immersion time in SBF.

The XRD pattern is shown in Fig. 7. The XRD peak of the silicon substrate can be detected but that of the ZrO_2 thin film cannot be found because the results are acquired by conventional diffractometry but not thin film diffractometry as used in the analysis of the ZrO_2 thin film. The XRD patterns of the ZrO_2 thin film soaked in SBF for 14 days are not shown here because the newly-formed Ca–P layer cannot yet be identified unambiguously. The reason is believed to be that the Ca–P layer is not yet crystallized to form apatite. After an immersion time of 28 days, the peaks of crystalline apatite can be easily identified in the XRD spectra indicating the formation of a new surface layer composed of crystalline apatite. The broadening of the peaks suggests that the apatite particles formed on the ZrO_2 thin film are superfine or have low crystallinity.

The FTIR spectra acquired from the ZrO_2 thin films immersed in SBF for 14 and 28 days are displayed in Fig. 8. Broad OH^- absorption bands from 3700 to 2500 cm^{-1} (Fig. 8a) and a weak water absorption band around 1650 cm^{-1} (Fig. 8b) can be seen in these spectra. The bands between 1400 and 1550 cm^{-1} (Fig. 8b) are due to the carbonate IR absorption v_3 [25]. The peak in the vicinity of

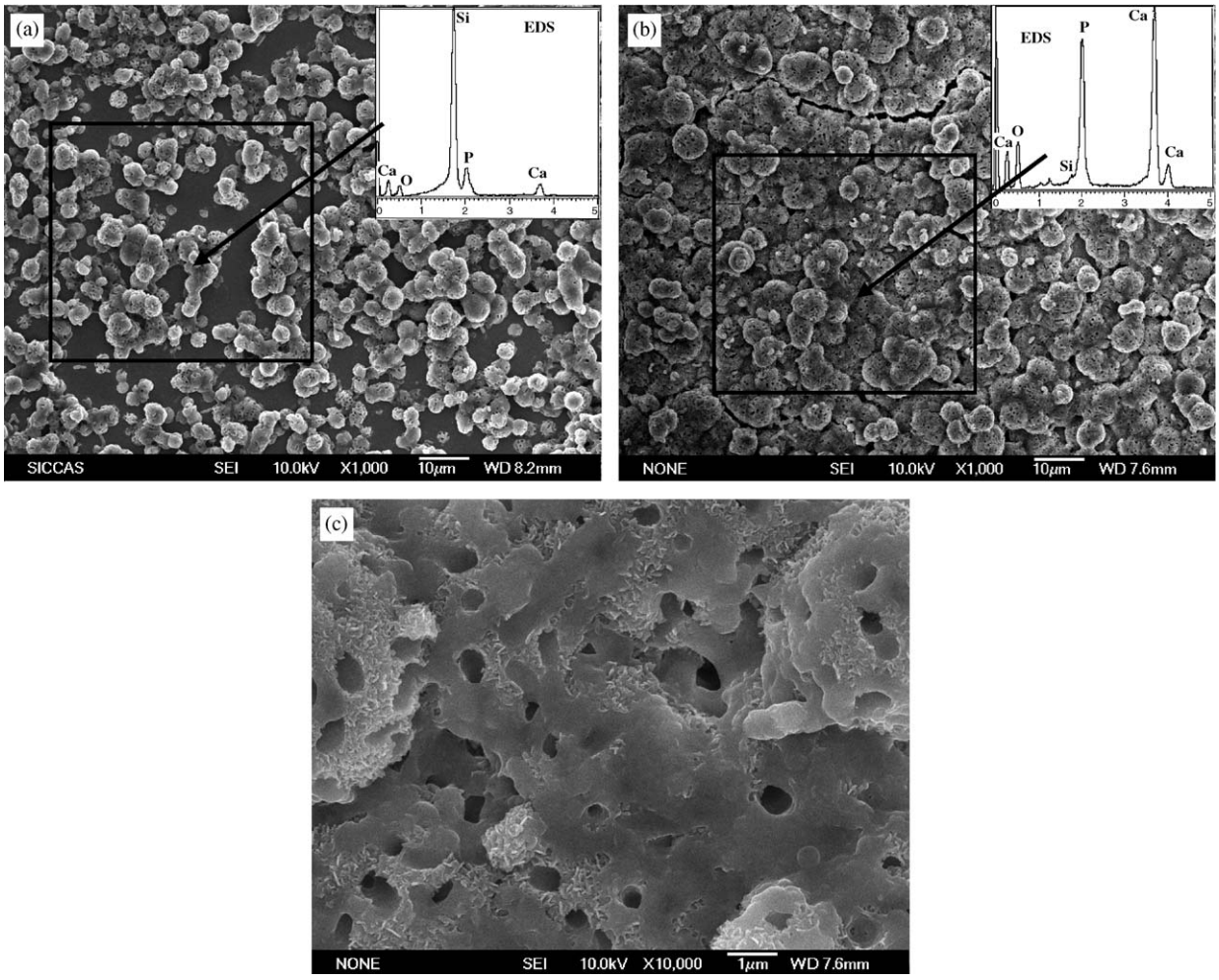

Fig. 6. SEM plan views and EDS spectra acquired from the ZrO_2 thin film soaked in SBF for (a) 14 days and (b) 28 days. A higher magnification view of the particles in (b) is shown in (c).

$870\,cm^{-1}$ (Fig. 8b) arises from both the carbonate and HPO_4^{2-} ions [26]. The broad band around $1100\,cm^{-1}$ (Fig. 8b) is mainly attributed to phosphate [26]. A sharp P–O bending mode doublet around $600\,cm^{-1}$ indicative of a crystalline phase of hydroxyapatite can also be observed in Fig. 8b [27]. The strong absorption peaks near 510 and $420\,cm^{-1}$ correspond to the Zr–O vibrational modes [23,24]. Our FTIR and TF-XRD results show that carbonate-containing hydroxyapatite (bone-like apatite) is formed on the tetragonal ZrO_2 thin films soaked in SBF, suggesting that the tetragonal ZrO_2 thin film is bioactive.

The HRTEM micrograph taken near the apatite and ZrO_2 thin film is depicted in Fig. 9. The picture shows that the apatite layer is in direct contact with the ZrO_2 thin film. In the HRTEM picture of the apatite, many disordered areas can be observed around the crystalline apatite indicating that the apatite layer on the ZrO_2 thin film has only partially crystallized. The (2 1 1) planes of the apatite with a spacing of about 0.28 nm are well resolved in this area. The HRTEM view of the ZrO_2 thin film shows that it also consists of nano-sized crystalline ZrO_2. It is worth noting that the outermost ZrO_2 crystal is smaller than that in the bulk of ZrO_2 thin film, as denoted in Fig. 9 by arrows. The size of the particles in the outermost layer is about several nanometers. It is believed to be one of the reasons why the ZrO_2 thin film is bioactive while other

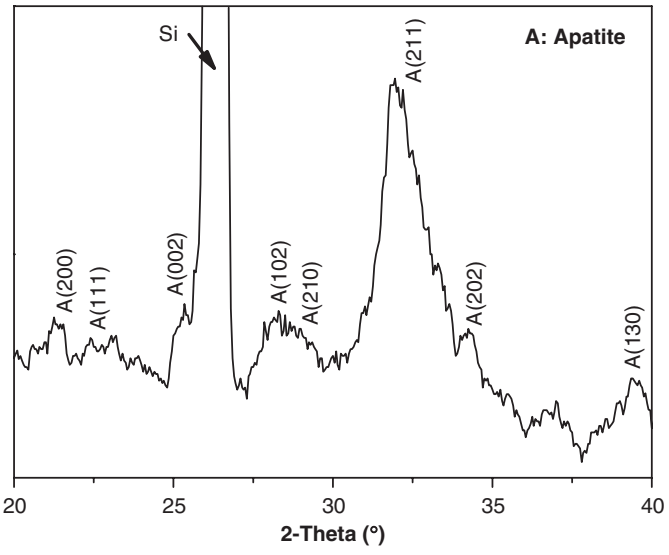

Fig. 7. XRD patterns of the ZrO_2 thin film soaked in SBF for 28 days.

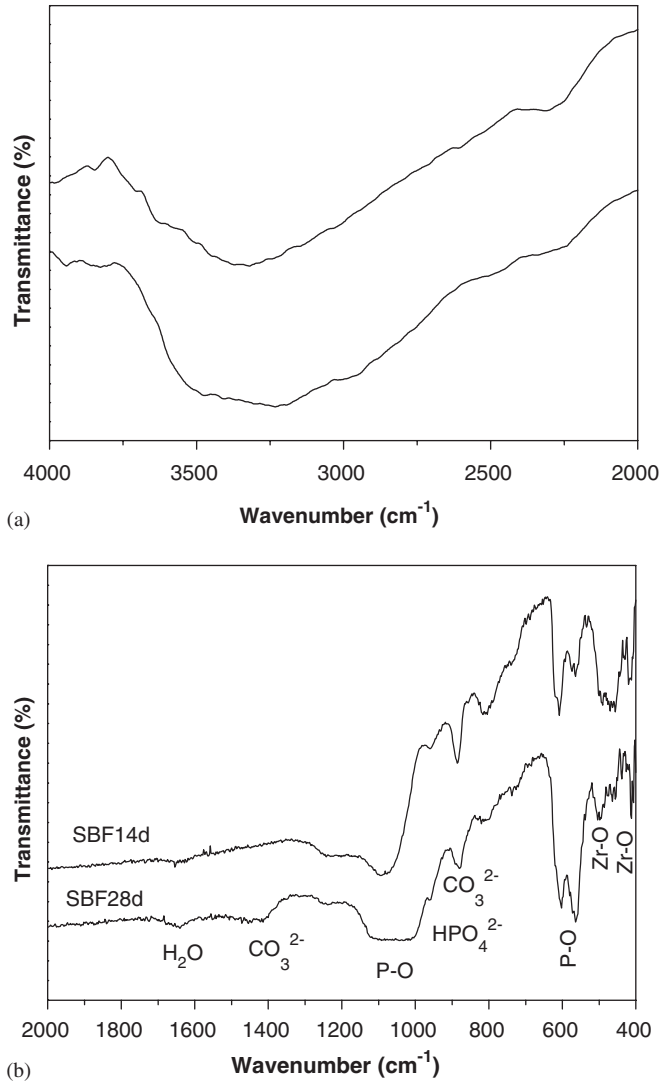

Fig. 8. FTIR spectra of the ZrO_2 thin film soaked in SBF for 14 and 28 days: (a) 4000–2000 $cm^{-1}$and (b) 2000–400 cm^{-1}.

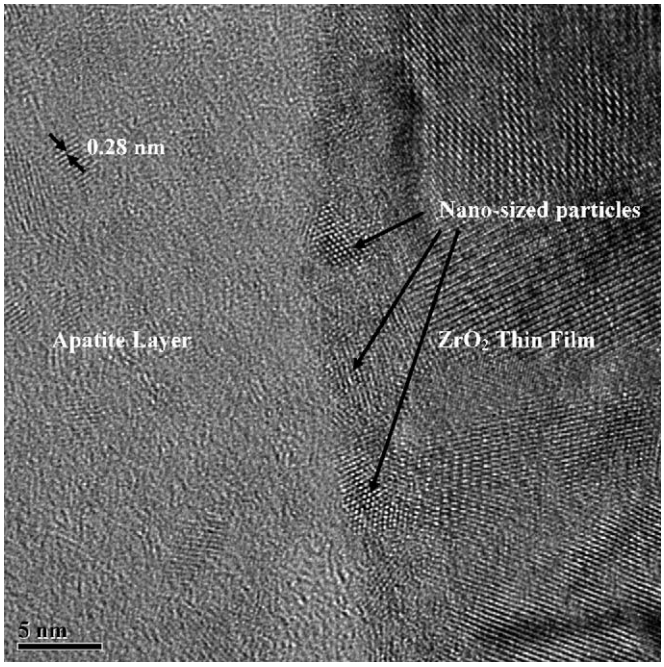

Fig. 9. High-resolution transmission electron microscopy (HRTEM) micrograph taken near the apatite and ZrO_2 thin film.

ZrO_2 materials such as ZrO_2 ceramic [6] and coatings [5] are bioinert. In our previous work, we have found that a TiO_2 coating with nano-sized surface can more easily induce apatite precipitation compared to a conventional TiO_2 surface [28]. The following mechanism is proposed to explain the improved surface bioactivity and additional experimental work is being performed in our laboratory to fathom the mechanism in details.

When the surface of an oxide ceramic is exposed to water in either the liquid or gaseous form, hydration occurs on its surface. These amphoteric MOH surface groups dissociate when the surface gets in contact with polar liquids. A surface charge of oxide materials can be achieved by two mechanisms which often act simultaneously: (i) dissociation of surface groups and (ii) adsorption of ions from the solution. The dissociation of amphoteric surface groups strongly depends on the pH of the solution and can be expressed by the following two equations [29]:

$$MOH + H^+ \leftrightarrow MOH_2{}^+ \leftrightarrow M^+ + H_2O, \quad (1)$$

$$MOH + OH^- \leftrightarrow M(OH)_2{}^- \leftrightarrow MO^- + H_2O. \quad (2)$$

While the first reaction gives rise to a positive charge, the second one produces a negative charge on the solid surface. There exists a certain pH at which the particles have no charge (or equal positive and negative charges), and this pH is called the isoelectric point (i.e.p.) or point of zero charge (p.z.c.). Moritz et al. [29] have indicated that the $pH_{(i.e.p.)}$ value of ZrO_2 ultra filtration is about 4.6. Its zeta-potential is about −30 mV when the pH of the solution is 7.4 which is equal to the pH of the SBF solution. Pettersson et al. [30] have also reported that the IEP of the pure monoclinic zirconia is about 6.4. Therefore, the surface charge of the ZrO_2 ceramic and thin film should be negative.

It is well known that the negatively-charged surface can attract calcium ions in the SBF solution to its surface. The deposition of calcium ions is the first and most crucial step of carbonate-containing hydroxyapatite nucleation from an ionic solution. This process is believed to initiate the growth of bone-like apatite on the surface of biocompatible implants [31]. The deposition of calcium ions is followed by the arrival of HPO_4^{2-} resulting in a hydrated precursor cluster consisting of calcium hydrogen phosphate. After the precursor clusters are formed, they spontaneously grow by consuming calcium and phosphate ions from SBF solution. The calcium phosphate phase is initially amorphous. It later crystallizes to a carbonate-containing hydroxyapatite

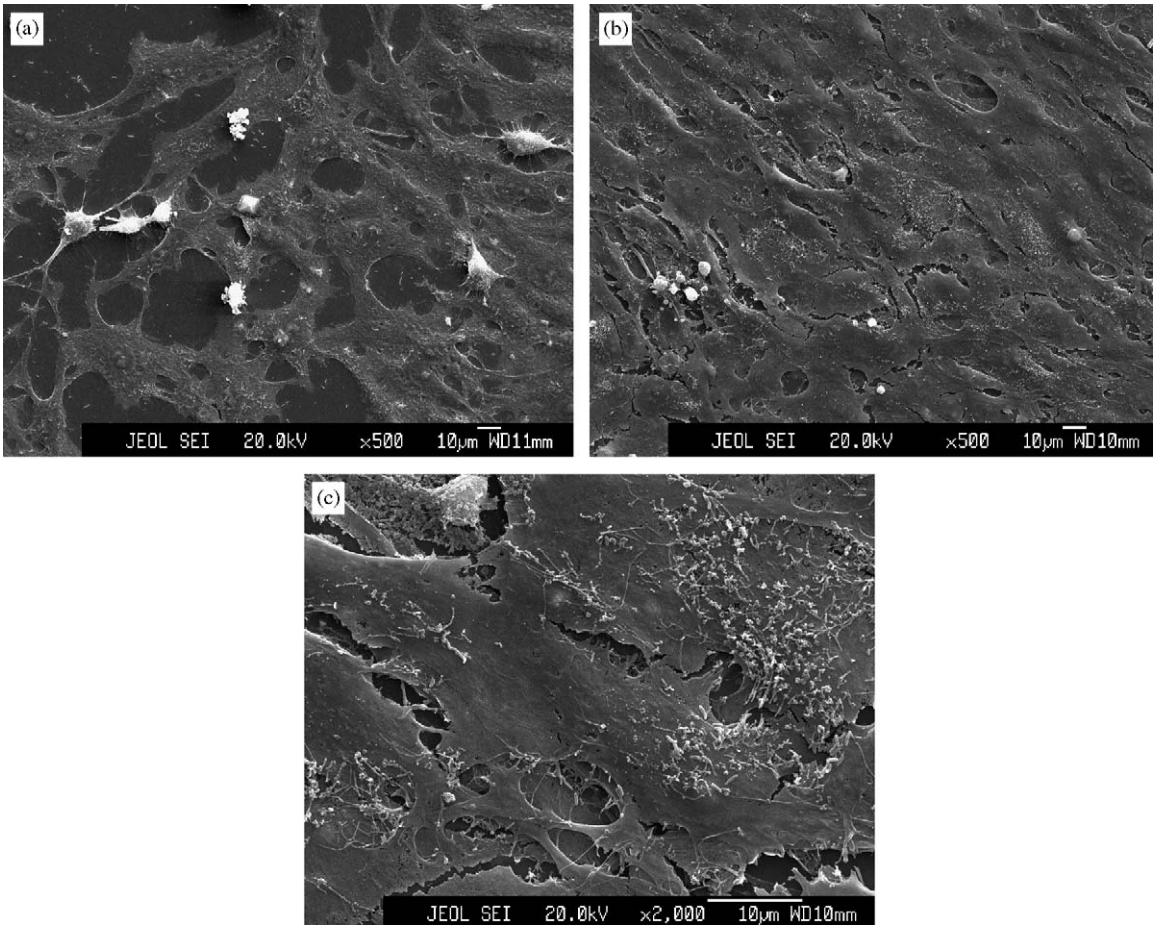

Fig. 10. BMMSC cells seeded on the ZrO_2 films after different times: (a) 1 day, (b) 4 days, and (c) higher magnification of (b).

structure by incorporating carbonate anions from the solution within the amorphous calcium phosphate phase.

The charge densities of the particles are determined by its size. Vayssieres et al. [32] have suggested that finer nanocrystalline particles have higher surface charge densities than larger ones. It can also be demonstrated by thermodynamic analysis that the surface or interfacial tension diminishes with decreasing particle size as a result of the increase in the potential energy of the bulk atoms of the particles [33]. Smaller particles with increased molar free energy are more likely to adsorb molecules or ions onto their surfaces in order to decrease the total free energy and to become more stable. Therefore, in this work, the nano-sized particles in the outermost layer of the ZrO_2 thin film may be the key factor to induce bone-like apatite to precipitate on its surface in SBF.

Fig. 10 exhibits the BMMSC cells seeded on the ZrO_2 films after different culture times. After 1 day, marrow stem cells are observed to grow and proliferate very well on the films surface (Fig. 10a). The surfaces are covered partially by the cells and extracellular matrix. With longer seeding time, the cells fuse to form a complete layer on the thin film surface (Fig. 10b). The higher magnification view shows that the cells possess good morphology with abundant dorsal ruffles and filapodia (Fig. 10c). Cell adhesion is involved in various natural phenomena such as embryogenesis, maintenance of tissue structure, wound healing, immune response, metastasis, as well as tissue integration with biomaterials. The biocompatibility of biomaterials is very closely related to the cell behavior in contact with them and particularly to cell adhesion to their surface. The surface characteristics of the materials such as the topography, chemistry, or surface energy, play an essential part in osteoblast adhesion. Thus, attachment, adhesion and spreading belong to the first phase of cell/material interactions and the quality of this first phase will influence the cell's capacity to proliferate and differentiate upon contact with the implant.

4. Conclusion

Tetragonal ZrO_2 thin films have been produced using a Zr filtered cathodic arc plasma source in the presence of an oxygen plasma. The thin film is composed of stoichiometric ZrO_2 (Zr:O = 1:2) and its composition is basically uniform throughout the thickness. Bone-like apatite is formed on the surface of the ZrO_2 thin film after it is soaked in SBF solution for a period of time. In the HRTEM micrograph of the apatite, many disordered areas can be observed around the crystalline apatite indicating that the apatite

layer on the ZrO_2 thin film has only partially crystallized. The cross-sectional HRTEM view obtained from the interface of the ZrO_2 thin film and apatite layer indicates that outermost layer of the thin film evolves from some nano-sized particles. These nanostructures are believed to be the key factor that induces precipitation of apatite on the surface. Bone marrow mesenchymal stem cells are observed to grow and proliferate in good states on the films surface. Our results suggest that the ZrO_2 thin film produced by this method is bioactive and cytocompatible.

Acknowledgements

This work was jointly supported by National Basic Research Fund under Grant 2005CB623901, Shanghai Science and Technology R&D Fund under Grants 0552nm014 and 03JC14074, Innovation Fund of SICCAS under Grant SCX200410, Foundation for the Author of National Excellent Doctoral Dissertation of PR China (FANEDD), and City University of Hong Kong Applied Research Grant no. 9667002. The authors thank Mr. Wanyin Zhai for technical assistance on the cell-culturing test.

References

[1] Piconi C, Maccauro G. Zirconia as a ceramic biomaterial. Biomaterials 1999;20:1–25.
[2] Chevalier J. What future for zirconia as a biomaterial? Biomaterials 2006;27:535–43.
[3] ISO TC 150/SC 1. Implants for surgery ceramic materials based on yttria-stabilized tetragonal zirconia (Y-TZP). ISO/DIS 13356, 1995.
[4] Yang YZ, Ong JL, Tian JM. Deposition of highly adhesive ZrO_2 coating on Ti and CoCrMo implant materials using plasma spraying. Biomaterials 2003;24:619–27.
[5] Liu XY, Ding CX. Bioactivity of plasma sprayed wollastonite/ZrO_2 composite coating. Surf Coat Technol 2003;172:270–8.
[6] Ferraris M, Verne HE, Appendino P, Moisescu C, Krajewski A, Ravaglioli A, et al. Coatings on zirconia for medical applications. Biomaterials 2000;21:765–73.
[7] Bosetti M, Verné E, Ferraris M, Ravaglioli A, Cannas M. In vitro characterisation of zirconia coated by bioactive glass. Biomaterials 2001;22:987–94.
[8] Gua YW, Yapb AUJ, Cheanga P, Khor KA. Effects of incorporation of HA/ZrO_2 into glass ionomer cement (GIC). Biomaterials 2005;26:713–20.
[9] Kim HW, Lee SY, Bae CJ, Noh YJ, Kim HE, Kim HM, et al. Porous ZrO2 bone scaffold coated with hydroxyapatite with fluorapatite intermediate layer. Biomaterials 2003;24:3277–84.
[10] Stanic V, Nicoli AN, Fini M, Giavaresi G, Giardino R, Krajewski A, et al. Osteointegration of bioactive glass-coated zirconia in healthy bone: an in vivo evaluation. Biomaterials 2002;23:3833–41.
[11] Uchida M, Kim HM, Kokubo T, Nawa M, Asano T, Tanaka K, et al. Apatite-forming ability of a zirconia/alumina nano-composite induced by chemical treatment. J Biomed Mater Res 2002;60:277–82.
[12] Uchida M, Kim HM, Kokubo T, Miyaji F, Nakamura T. Apatite formation on zirconium metal treated with aqueous NaOH. Biomaterials 2002;23:313–7.
[13] Uchida M, Kim HM, Kokubo T, Tanaka K, Nakamura T. Structural dependence of apatite formation on zirconia gel in simulated body fluid. J Ceram Soc Japan 2002;110:710–5.
[14] Dobson KD, McQuillan AJ. An infrared spectroscopic study of carbonate adsorption to zirconium dioxide sol–gel films from aqueous solutions. Langmuir 1997;13:3392–6.
[15] Fang MM, Kaschak DM, Sutorik AC, Mallouk TE. A "mix and match" ionic-covalent strategy for self-assembly of inorganic multilayer films. J Am Chem Soc 1997;119:12184–91.
[16] Zhu NN, Zhang AP, Wang QJ, He PG, Fang YZ. Electrochemical detection of DNA hybridization using methylene blue and electrodeposited zirconia thin films on gold electrodes. Anal Chim Acta 2004;510:163–8.
[17] Liu SQ, Xu JJ, Chen HY. ZrO_2 gel-derived DNA-modified electrode and the effect of lanthanide on its electron transfer behavior. Bioelectrochemistry 2002;57:149–54.
[18] Zhang T, Chu PK, Brown IG. Effects of cathode materials and arc current on optimal bias of a cathodic arc through a magnetic duct. Appl Phys Lett 2002;80:3700–2.
[19] Kokubo T, Kushitani H, Sakka S, Kitsugi T, Yamamuro T. Solutions able to reproduce in vivo surface-structure changes in bioactive glass-ceramic A-W. J Biomed Mater Res 1990; 24:721–34.
[20] Maniatopoulos C, Sodek J, Melcher AH. Bone formation in vitro by stromal cells obtained from bone marrow of young adult rats. Cell Tissue Res 1988;254:317–30.
[21] Hirst RA, Yesilkaya H, Clitheroe E, Rutman A, Dufty N, Mitchell TJ, et al. Sensitivities of human monocytes and epithelial cells to pneumolysin are different. Infect Immun 2002;70:1017–22.
[22] Méndez-Vivar J, Mendoza-Serna R, Valdez-Castro L. Control of the polymerization process of multicomponent (Si,Ti,Zr) sols using chelating agents. J Non-Cryst Solids 2001;288:200–9.
[23] Phillippi CM, Mazdiyasni KS. Infrared and Raman spectra of zirconia polymorphs. J Am Ceram Soc 1971;54:254–8.
[24] Pecharroman C, Ocan M, Sena CJ. Optical constants of tetragonal and cubic zirconias in the infrared. J Appl Phys 1996; 80:3479–83.
[25] Nakamoto K. Infrared and Raman spectra of inorganic and coordination compounds. New York: Wiley; 1986. p. 124.
[26] Weng J, Liu Q, Wolke JGC, Zhang X, de Groot K. Formation and characteristics of the apatite layer on plasma-sprayed hydroxyapatite coatings in simulated body fluid. Biomaterials 1997; 18:1027–35.
[27] Canham LT, Reeves CL. Apatite nucleation on low porosity silicon in acellular simulated body fluid. In: Cotell CM, Meyer AE, Gorbatkin SM, Grobe III GL, editors. Thin films and surfaces for bioactivity and biomedical applications: symposium held November 28–29, 1995, Boston, MA, USA, Pittsburgh: Materials Research Society; 1996. p. 189–194.
[28] Liu XY, Zhao XB, Fu RKY, Ho JPY, Ding CX, Chu PK. Plasma-treated nanostructured TiO_2 surface supporting biomimetic growth of apatite. Biomaterials 2005;26:6143–50.
[29] Moritz T, Benfer S, Árki P, Tomandl G. Influence of the surface charge on the permeate flux in the dead-end filtration with ceramic membranes. Separ Purif Technol 2001;25:501–8.
[30] Pettersson A, Marino G, Pursiheimo A, Rosenholm JB. Electrosteric stabilization of Al_2O_3, ZrO_2, and 3Y-ZrO_2 suspensions: effect of dissociation and type of polyelectrolyte. J Colloid Interface Sci 2000;228:73–81.
[31] Svetina M, Ciacchi LC, Sbaizero O, Meriani S, De Vita A. Deposition of calcium ions on rutile (1 1 0): a first-principles investigation. Acta Mater 2001;49:2169–77.
[32] Vayssières L, Chanéac C, Trone E, Joliver JP. Size tailoring of magnetite particles formed by aqueous precipitation: an example of thermodynamic stability of nanometric oxide particles. J Colloid Interface Sci 1998;205:205–12.
[33] Zhang H, Penn RL, Hamers RJ, Banfield JF. Enhanced adsorption of molecules on surfaces of nanocrystalline particles. J Phys Chem B 1999;103:4656–62.